Article

Enhanced Photocatalytic Activity of ZnWO Catalyst via Fluorine Doping

Guangli Huang, and Yongfa Zhu

J. Phys. Chem. C, **2007**, 111 (32), 11952-11958• DOI: 10.1021/jp071987v • Publication Date (Web): 21 July 2007

Enhanced Photocatalytic Activity of $ZnWO_4$ Catalyst via Fluorine Doping

Guangli Huang and Yongfa Zhu*

Department of Chemistry, Tsinghua University, Beijing 100084, P. R. China

Received: March 12, 2007; In Final Form: May 15, 2007

Fluorine interstitially doped $ZnWO_4$ ($F-ZnWO_4$) was synthesized by fluorine-ion addition in a hydrothermal process. The effects of fluorine doping on crystal structure, optical properties, and photocatalytic activity of $ZnWO_4$ catalyst were investigated. The results showed that the doped fluorine ions could increase the coordination sphere around the W atom in a WO_6 octahedron and cause the distortion of the WO_6 octahedron in a $ZnWO_4$ crystal. Moreover, the strength of absorption in the UV region and transfer rate of photogenerated electrons to the surface increased after doping with fluorine. With an increase of fluorine doping concentration, the photoactivities of samples were enhanced greatly. The photocatalytic activity can be enhanced 2.6 times for the degradation of RhB when the optimal atomic ratio of F/Zn was 0.4. The enhanced photocatalytic activity originated from the increase of transfer rate of photogenerated electrons to the photocatalyst surface.

1. Introduction

Photocatalytic reactions of semiconductors, such as splitting of water and degradation of organic and inorganic pollutants, have been receiving great attention.[1,2] Recently, $ZnWO_4$, one of the important photocatalysts, has been used for water splitting and mineralization of organic pollutants under UV irradiation.[3−6] However, its industrial application is hampered because the photocatalytic activity of $ZnWO_4$ is not high enough for the requirements of practical application.[5] Therefore, it is still a principal challenge to enhance the photocatalytic activity of $ZnWO_4$. A few researchers have reported that the photocatalytic activity of semiconductor photocatalysts can be improved by surface fluorine modification or fluorine doping.[7−16] Minero et al. found that surface fluorination enhanced the photocatalytic activity of TiO_2 powders.[7−9] Choi et al. investigated effects of surface fluorides on TiO_2 in the photocatalytic oxidation of different substrates and confirmed that the high photocatalytic activities of $F-TiO_2$ samples were due to the enhancement of the OH-radical-mediated oxidation pathways.[10] In these cases, the added fluorine ions existed only on the surface of TiO_2. Recently, high photocatalytic activity for decomposition of gas-phase acetone was obtained by lattice fluorine doping in the TiO_2 photocatalyst; the explanation for this enhancement is that doped F^- converts some Ti^{4+} to Ti^{3+}, which slows down the recombination of the electron−hole pairs.[11] Li et al. further confirmed that photocatalytic activity of fluorine-doped TiO_2 increased for the decomposition of gas-phase acetaldehyde.[12] Meanwhile, enhanced photocatalytic activity on TiO_2 films by fluorine introduction was also researched; the reason for the promoting effect is the improvement of the anatase crystallinity caused by fluorine ions.[13,14] Moreover, a few fluorine-doped non-TiO_2 catalysts also exhibited a similar enhancement of photocatalytic activities. Fluorine-doped $SrTiO_3$ showed about three times the photocatalytic activity compared with that of pure $SrTiO_3$. The formation of oxygen vacancies and increase of effective electron mobility were the main reasons.[15,16] On the basis of these results, it can be inferred that the introduction of fluorine, irrespective of the approaches of fluorine doping, really enhanced the photocatalytic activity of semiconductor photocatalysts.

Up to now, there are no reports on the photocatalytic activity of fluorine-doped $ZnWO_4$, although the luminescent properties of $ZnWO_4$ can be improved by doping with fluorine.[17] In this work, fluorine interstitially doped $ZnWO_4$ samples with different fluorine concentrations were synthesized by a hydrothermal process. Our principal aim is to investigate the role of fluorine introduction on the structure, optical properties, and photocatalytic activity of the $ZnWO_4$ catalyst. The effects of fluorine on expediting the photocatalytic activity of a $ZnWO_4$ catalyst have been discussed in detail.

2. Experiment Section

2.1. Synthesis of Doped Samples. Fluorine-doped $ZnWO_4$ samples were prepared through a hydrothermal process. All chemicals used were analytic grade reagents without further purification. $Zn(NO_3)_2 \cdot 6H_2O$ and $Na_2WO_4 \cdot 2H_2O$ (1:1 molar ratio) were mixed together, and then 100 mL of distilled water was added. White precipitates appeared immediately, and the beaker was placed in an ultrasonic bath for 30 min to complete the precipitation reaction. The precipitates were filtered off, washed several times with distilled water, and then added to stainless steel autoclaves with a Teflon liner containing a mixed solution of 30 mL of distilled water and desired amounts of NH_4F. In what follows, the value of R_F is used to describe the atomic ratio of F to Zn; these were 0, 0.1, 0.2, 0.4, 0.8, 1.0, and 3.0 nominal atomic ratios in the synthesis solution. After being sealed, the autoclaves were heated in a convection oven at 180 °C for 24 h. The products were collected by filtration and then were washed by distilled water several times until no F^- was left in the solution as tested. The samples were then dried at 80 °C for 4 h before characterization.

2.2. Characterization. The products were characterized by powder X-ray diffraction (XRD) on a Bruker D8-advance X-ray diffractometer at 40 kV and 40 mA for monochromatized Cu Kα (λ = 1.5418 Å) radiation. Morphologies of the prepared samples were further examined with transmission electron microscopy (TEM) by a JEM 1200 electron microscope operated

* Author to whom correspondence should be addressed. Tel: +86-10-62783586. Fax: +86-10-62787601. E-mail: zhuyf@tsinghua.edu.cn.

10.1021/jp071987v CCC: $37.00
Published on Web 07/21/2007

at an accelerating voltage of 100 kV. The Brunauer−Emmett−Teller (BET) surface area was determined by ASAP 2010 V5.02H. The adsorbed gas was nitrogen. The X-ray photoelectron spectroscopy (XPS) analysis was conducted on a PHI 5300 ESCA instrument using an Al Kα X-ray source at a power of 250W. The atomic ratio in the sample was further determined with a sequential X-ray fluorescence spectrometer (XRF-1700, Shimadzu). Infrared transmission spectra were recorded for KBr disks containing the powder sample with a FT-IR spectrometer (Perkin-Elmer 1600). The intermediates were quantified by a HPLC (Agilent 1100) system using an ammonium phosphate buffer solution (0.1%, v/v) and methanol as eluent (from 60% to 90% methanol over 15 min), and the flow rate was 1 mL/min. A C-18 reverse-phase column was employed. UV−vis diffuse reflectance spectra (DRS) of the samples were measured by using a Hitachi U-3010 UV−vis spectrophotometer.

2.3. Photocurrent Measurement. Photocurrent measurements were performed by using a CHI 660B electrochemical workstation. For photocurrent measurements, 25 mg of photocatalyst was suspended in distilled H_2O (75 mL) containing acetate (0.1 M) and Fe^{3+} (0.1 mM) as an electron donor and acceptor, respectively, and the pH value of the suspension was adjusted to 1.5 with $HClO_4$. A Pt plate (1×1 cm^2, 0.125 mm thick, both sides exposed to solution), a saturated calomel electrode (SCE), and a Pt gauze were immersed in the reactor as working (collector), reference, and counter electrodes, respectively. With continuous Ar purging of the suspension, photocurrents were measured by applying a potential (+0.6 V vs SCE) to the Pt electrode using a potentiostat (EG&G). All experiments were conducted at 27 ± 2 °C.

2.4. Photocatalytic Test. Photocatalytic activities of samples were evaluated by degradation of rhodamine-B (RhB) under ultraviolet light irradiation of an 11 W low-pressure lamp with 254 nm. The photocatalytic reactive system is shown in the Supporting Information (Figure S1). The average light intensity was 0.9 mW/cm^2. The radiant flux was measured with a power meter from the Institute of Electric Light Source (Beijing). RhB solutions (200 mL, 1.0×10^{-5} mol L^{-1}) containing 0.10 g of as-prepared samples were placed in a glass beaker. Before the light was turned on, the solution was first ultrasonicated for 10 min, and then stirred for 10 min to ensure equilibrium between the catalysts. Volumes of 3 mL of sample solutions were taken at given time intervals and separated through centrifugation (4000 rpm, 10 min). The supernatants were analyzed by recording variations of the absorption band maximum (553 nm) in the UV−vis spectra of RhB using a U-3010 spectrophotometer (Hitachi).

3. Results

3.1. Chemical States of Fluorine Doped in the Photocatalyst. Figure 1A shows XRD patterns of $ZnWO_4$ catalysts with different fluorine concentrations. It illustrates that doping with fluorine does not result in the development of new crystal orientations or changes in preferential orientations. Hence, independently of the presence or absence of fluorine, the samples are constituted of pure monoclinic $ZnWO_4$ phase. However, a careful comparison of the (100) diffraction peaks in the range of $2\theta = 18-20°$ (Figure 1B) shows that the peak position of $ZnWO_4$ with different fluorine contents shifts slightly toward a lower 2θ value. The same results are also presented in other diffraction peaks. According to Bragg's law,

$$d_{(hkl)} = \lambda/(2 \sin \theta)$$

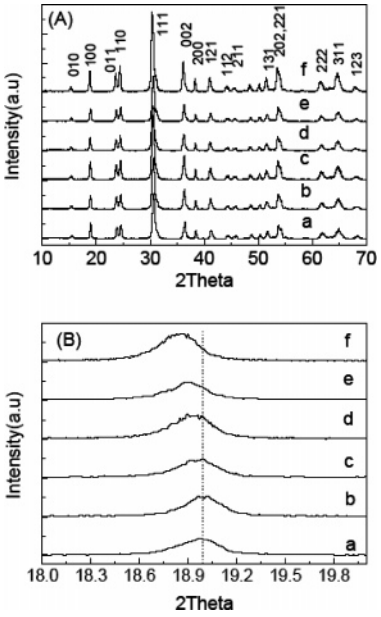

Figure 1. (A) XRD patterns of the samples prepared from NH_4F-H_2O mixed solution with different R_F values at 180 °C for 24 h. (a) 0, (b) 0.1, (c) 0.2, (d) 0.4, (e) 0.8, (f) 1.0. (B) Diffraction peak positions of the (100) plane in the range of $2\theta = 18-20°$.

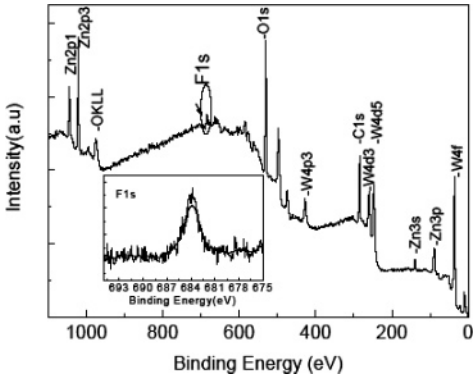

Figure 2. XPS survey spectrum of fluorine-doped $ZnWO_4$ samples prepared by a hydrothermal method in NH_4F-H_2O mixed solution with $R_F = 3.0$ at 180 °C for 24 h. The inset is the F 1s peak intensity of an as-prepared sample with $R_F = 3.0$.

where $d(hkl)$ is the distance between crystal planes of (hkl), λ is the X-ray wavelength, and θ is the diffraction angle of the crystal plane (hkl). Because the ionic radius of F^- (0.133 nm) is smaller than that of O^{2-} (0.140 nm), the decrease in lattice parameters ($d(hkl)$ value) should result in the increase in 2θ values. Therefore, the observed shift of diffraction peak toward lower angles is not due to the smaller lattice parameter expected for substitution of O^{2-} by F^-. Instead, this may be due to an increase in lattice parameter by repulsion between F^- anions which may occur as interstitial dopants. On this basis, the observed shift in 2θ indicates interstitial doping with F^- ions.

Figure 2 shows an XPS survey spectrum of fluorine-doped $ZnWO_4$ catalyst with $R_F = 3.0$ (nominal atomic ratio). It indicates that the $F-ZnWO_4$ samples are mainly composed of Zn, W, O, and F elements and a trace amount of carbon. Quantitative analysis demonstrates that the atomic ratio of Zn/W/O/F is 1:1.2:5.5:0.4, which is not in agreement with the nominal atomic ratio of $ZnWO_4$. XRF was further used to determine the atomic ratio of F/Zn. Quantitative results give the atomic ratio of 0.5 for F/Zn when the nominal atomic ratio is 3.0. It is close to the result of XPS. An XPS spectrum of the F 1s peak is shown in the inset of Figure 2. The binding energy

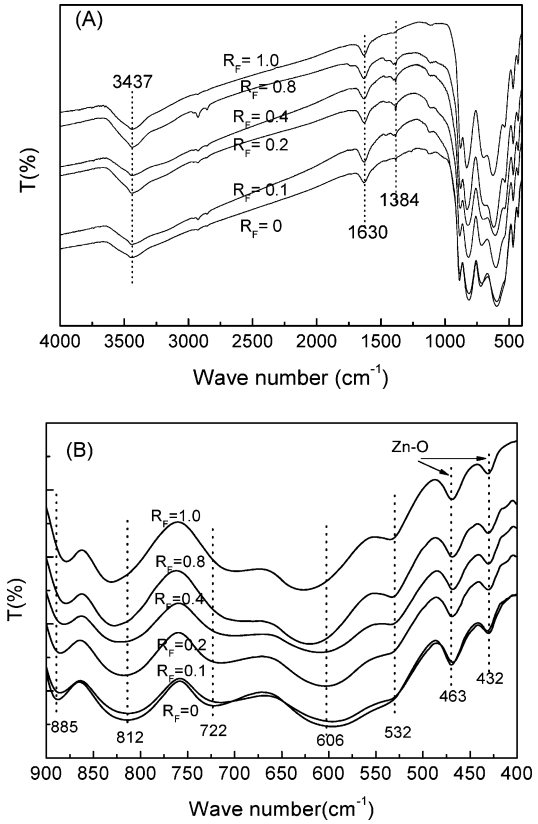

Figure 3. (A) FT-IR spectra of $ZnWO_4$ catalysts with different fluorine-doped concentrations. (B) A careful comparison in the range of 900−400 cm^{-1}.

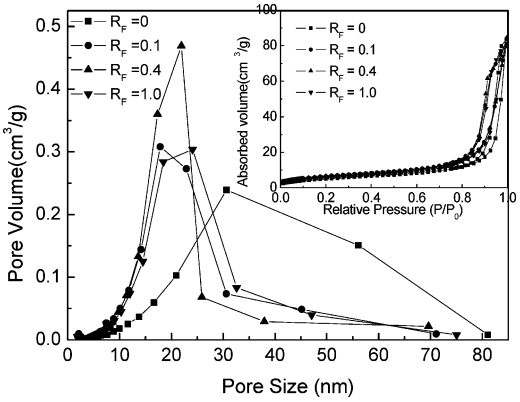

Figure 4. Pore size distribution curve calculated from the desorption branch of the nitrogen isotherm by the BJH method and corresponding nitrogen adsorption−desorption isotherms (inset) of F−$ZnWO_4$ samples prepared by a hydrothermal method in NH_4F− H_2O mixed solution at 180 °C for 24 h.

TABLE 1: Effect of R_F on Crystal Size and Specific Surface Areas of As-Prepared Samples

R_F[a]	crystal size[b] (nm)	specific surface area (m^2/g)
0	25.3	20.0
0.1	27.8	24.7
0.4	27.2	24.8
1.0	27.1	23.6

[a] Nominal molar ratios of NH_4F to $ZnWO_4$. [b] Crystal size of the samples calculated by the Scherrer equation: $D_c = K\lambda/(\beta \cos \theta)$ using the parameters of the (002) peak.

of F 1s is at 684.1 eV. Generally, the F 1s binding energy of 684 eV corresponds to the fluorine ions adsorbed on TiO_2, and that of 688 eV corresponds to the fluorine ions in the lattice.[10,11] However, according to the results of $Cs_2WO_2F_4$[18] and XRD, the F 1s binding energy of 684.1 eV corresponds to the fluorine ions in the interstitial lattice. The XPS survey spectra of other as-prepared samples are similar. Therefore, it can be inferred that the contribution of the F 1s peak is fluorine ions in the interstitial lattice of the $ZnWO_4$ crystal.

Figure 3 shows FT-IR spectra of $ZnWO_4$ catalysts with different fluorine doping concentrations. In Figure 3A, the bands at 3300−3600 cm^{-1} and 1630 cm^{-1} are attributed to an OH stretching vibration, and the band at 1384 cm^{-1} corresponds to the bending mode of OH groups. The peaks in the range of 900−400 cm^{-1} are assigned to the stretching vibrations of $ZnWO_4$.[19] The bending and stretching vibrations of Zn−O (the oxygen from W−O−W linkage) occur at 432 and 463 cm^{-1}. The bands corresponding to W−O bond stretching and bending vibrations in WO_6 group occur at 885, 812, 722, 606, and 532 cm^{-1}. A careful comparison of IR peaks in the region 900−400 cm^{-1} is presented in Figure 3B. With the increase of fluorine concentration, the shape and location of peaks of Zn−O vibrations at 432 and 463 cm^{-1} are unchanged, but the location of peaks of W−O vibrations are changed. The bands at 606 and 812 cm^{-1} shift to higher wavenumber, and the bands at 722 and 885 cm^{-1} shift to lower wavenumber. Moreover, the bands at 532 cm^{-1} are also related to vibrations of W−O, the strength of which increases with an increase of fluorine doping concentration. Therefore, it can be speculated that the increase in the bands at 606 and 812 cm^{-1} and the decrease in the bands at 722 and 885 cm^{-1} could be related to the change in the coordination sphere around the W atom.[17] The $ZnWO_4$ structure comprises infinite zigzag chains, running parallel to [001], of either an edge-sharing WO_6 octahedron or an edge-sharing ZnO_6 octahedron. Each chain of the ZnO_6 octahedron is corner-linked to four chains of WO_6 and vice versa, leaving open channels which are also parallel to [001].[20] On the basis of the above observations, the interstitially doped fluorine may influence the coordination sphere around the W atom, so the distortion of the WO_6 octahedron may exist in the $ZnWO_4$ structure.

3.2. Pore Structure and Specific Surface Area. Figure 4 shows the pore size distribution curve calculated from the desorption branch of the nitrogen isotherm by the BJH method. It shows that the peak pore sizes of as-prepared samples are singlet, indicating that the pore is arising from the aggregates of as-prepared samples. The peak shifts toward the left after the sample is doped with fluorine in Figure 4. The peak pore size of the interparticles shifts to the left, indicating that decrease of pores. It means that the crystallinity of $ZnWO_4$ is improved, which is consistent with results of ref 11. In general, the pore size decreased after $ZnWO_4$ is doped by fluorine, then increased after $ZnWO_4$ was doped with $R_F = 0.4$. But in the range from 0.1 to 1.0, the pore size of doped samples changes a little.

The specific surface areas of as-prepared samples are listed in Table 1. For fluorine-doped $ZnWO_4$ samples, the surface areas increase with an increase of fluorine doping concentration up to a maximum of 0.4 and then change a little with an increase of fluorine concentration, elucidating that a certain amount of fluorides can inhibit some particles interconnected with each other.

3.3. Crystal Size and Morphology. Figure 5 shows TEM photographs of $ZnWO_4$ catalysts with different fluorine concentrations. Images show that the morphologies of as-prepared samples are homogeneous, indicating that fluorine does not change the morphologies of $ZnWO_4$. It also can be found that the particle size (∼30 nm) of fluorine-doped $ZnWO_4$ (Figure

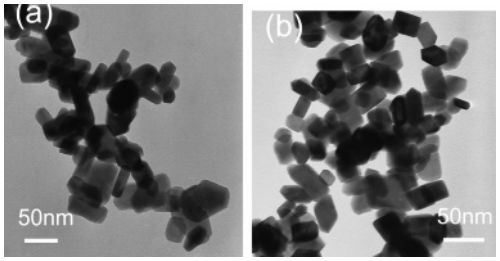

Figure 5. TEM photographs of $ZnWO_4$ samples with different F amounts. (a) $R_F = 0$; (b) $R_F = 0.4$.

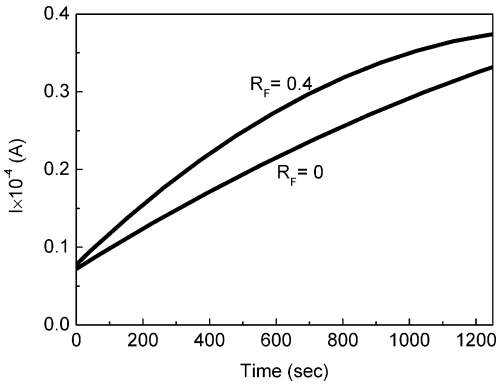

Figure 6. Photocurrent generated with UV irradiation time over doped and undoped samples suspended with acetate and Fe^{3+}.

5b) is similar to that of pure $ZnWO_4$ (Figure 5a) prepared under the same conditions, which is in good agreement with the value determined by XRD (27.2 and 25.3 nm) in Table 1. For $ZnWO_4$ with $R_F = 0.1$, the crystal size increases to 27.8 nm, which is due to the fact that the F^- ions slightly promote crystallization of $ZnWO_4$. In the R_F range from 0.1 to 1.0, the crystal sizes of the samples are almost the same.

3.4. Photocurrent Investigation. Endo et al.[21] claimed that effective electron mobility in the conduction band would increase with the increasing of F^- content. So the photogenerated electrons could easily diffuse from the inner regions to the surface of the grains to take the function of redox.[15,16] The mobility capability of electrons generated in the photocatalyst can be directly monitored by the photocurrent, and the rate should directly correlate with the photocatalytic activity of the material.[22] Figure 6 shows the photocurrent of samples generated in suspensions under UV light. It is noted that the photocurrent of $ZnWO_4$ with $R_F = 0.4$ is approximately 1.2 times larger than that of an undoped $ZnWO_4$ sample. This indicates that CB electron transfer to Fe^{3+} is faster on fluorine-doped $ZnWO_4$ than on undoped $ZnWO_4$.[22] Therefore, it can be concluded that fluorine doping promotes the transfer rate of electrons to the photocatalyst surface.

3.5. Photoabsorbance Property. The UV−vis diffuse reflectance spectra of fluorine-doped samples are shown in Figure 7. It shows that the samples with different amounts of fluorine present almost the same absorption edges, except that the absorption edge of samples with $R_F = 0.4$ and $R_F = 0.8$ display slightly a red-shift. It is more accurate for the determination of the band gap energy E_g of a semiconductor using the following equation: $a = A((h\nu - E_g)^{n/2})/(h\nu)$, where a, υ, E_g, and A are absorption coefficient, light frequency, band gap, and a constant, respectively. Among them, n depends on whether the transition is direct ($n = 1$) or indirect ($n = 4$).[23] The optical transition for $ZnWO_4$ is directly allowed, so the value of n for $ZnWO_4$ is 1.[5,24] Therefore, the band gaps of samples with different R_F values (0−1.0) are estimated to be 3.69, 3.70, 3.72, 3.60, 3.63,

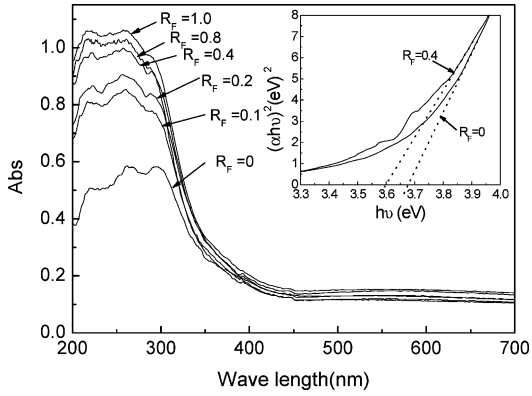

Figure 7. UV−vis diffuse reflectance spectra of $ZnWO_4$ samples with different R_F values.

and 3.68 eV from the $(ah\nu)^{2/n}$ versus $h\nu$ plots, respectively.[3,4] Furthermore, the fluorine-doped samples present stronger absorption in the UV range than the undoped $ZnWO_4$ sample. It was due to doping with fluorine ions.[11] The absorption of $ZnWO_4$ under UV regions was assigned to the band transition from the occupied O 2p orbital to the empty W 5d orbital.[5] Moreover, the interstitial doping of fluorine ions could increase the coordination sphere around the W atom in a WO_6 octahedron.[17] On the basis of the above results, it is reasonable to infer that the optical transitions are comprised of the d^0 orbitals of W and the 2p orbitals of O and F. This conclusion is similar to the result of fluorine-doped TiO_2 reported by Hattori et al.,[25] who claimed that doped fluorine can contribute to the optical absorption of TiO_2.

3.6. Photocatalytic Activity. The photocatalytic performances of the $ZnWO_4$ samples doped with different fluorine concentrations were investigated by the decomposition of RhB aqueous solution under UV irradiation (Figure 8). In Figure 8A, the concentration of RhB initially decreases originally from ultrasonic. After that, the adsorption of RhB on the $ZnWO_4$ undoped sample and $ZnWO_4$ samples with $R_F = 0.4$ is similar. The RhB photodegradation over the $ZnWO_4$ catalyst is fitted for pseudo-first-order kinetics.[4,5] Figure 8B shows that the doped samples exhibit higher photocatalytic activities than the undoped sample. The blank test confirms that RhB cannot be degraded in the dark and can only be slightly degraded under UV light without catalysts, indicating that the photolysis and adsorption of catalysts can be ignored. The sample of $R_F = 0$ shows decent photocatalytic activity with a rate constant k of 1.77×10^{-2} min^{-1}. The photocatalytic activities of samples increase with an increase of doped fluorine concentration. It is amazing that over 90% of RhB is degraded after 60 min irradiation. The k reaches the highest value of 4.56×10^{-2} min^{-1}, which raises 2.6 times compared with that of the undoped sample, when R_F is 0.4. However, with further increase of doped fluorine concentration, the photocatalytic activity of as-prepared samples decreases, and finally reaches 2.02×10^{-2} min^{-1} when R_F is 1.0. The 4-chlorophenol photocatalytic degradation over as-prepared samples displays similar results (Supporting Information, Figure S2).

Figure 9 presents the temporal evolution of the spectral changes during the photodegradation of RhB over $ZnWO_4$ with $R_F = 0$, $R_F = 0.4$, and HPLC chromatogram (inset) of RhB solution at various time intervals for the photocatalytic degradation process. On the basis of the results of ref 26, the diminishment of the absorption band of RhB at 553 nm demonstrates decomposition of the conjugated xanthene ring in RhB; a hypsochromic shift of the band is due to the stepwise

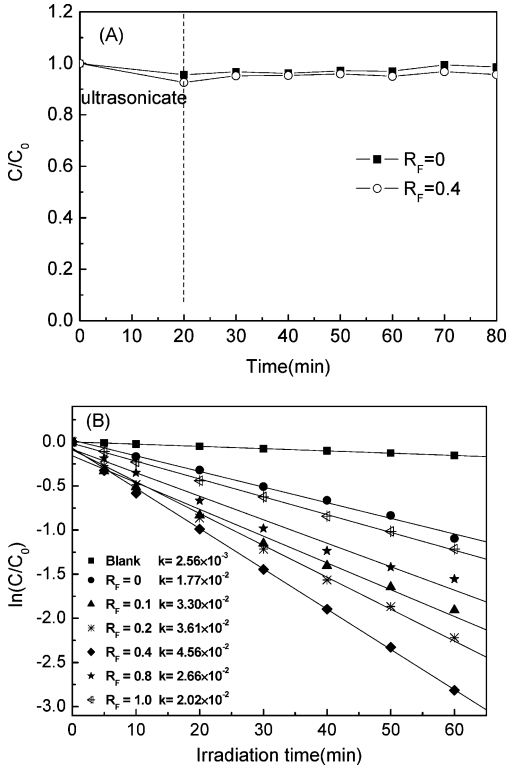

Figure 8. (A) The adsorption of RhB on undoped $ZnWO_4$ and doped $ZnWO_4$ samples in the dark are compared. (B) The photocatalytic activities of various samples with different amounts of doped fluorine, catalyst loading, 0.50 g L^{-1}; RhB, 1.0×10^{-5} mol L^{-1}.

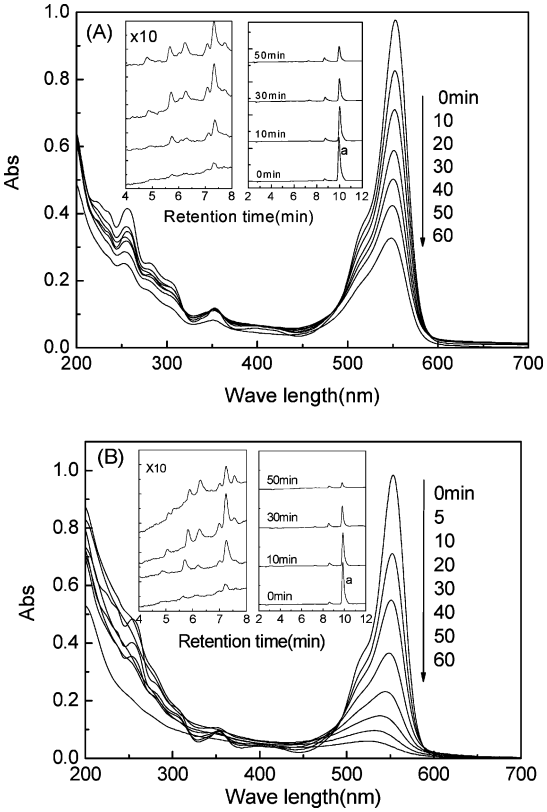

Figure 9. Temporal evolution of the spectral changes during the photodegradation of RhB over $ZnWO_4$ with different doped fluorine concentrations and HPLC chromatograms (inset) of RhB solution at various time intervals for the photocatalytic degradation process, (A) $R_F = 0$, (B) $R_F = 0.4$.

de-ethylation of the *N*,*N*′-diethylammonium groups in the RhB structure. In the case of $ZnWO_4$ catalyst with $R_F = 0.4$ (Figure 9B), the characteristic absorption band of the dye (around 553 nm) decreases rather rapidly when compared to the photodegradation of undoped $ZnWO_4$ (Figure 9A). In addition, no obvious shift of absorbance at 553 nm is observed during the photocatalytic process as selectively shown in Figure 9A and Figure 9B. In the HPLC chromatogram (inset of Figure 9A), the peak with a retention time of 10 min is attributed to the initial RhB dye, and other peaks correspond to intermediates. The degradation process of RhB is in good agreement with that of its photoelectrocatalytic oxidation at a $ZnWO_4$ film.[3] It can be seen that the peak *a* disappeared quickly and the other peaks slightly increased, which proved that the efficient decomposition of the conjugated xanthene ring in RhB occurred. The sample with $R_F = 0.4$ (in Figure 9B) presents results similar to those of undoped $ZnWO_4$. Moreover, a careful comparison of the range from 4 to 8 min shows that the degradation process of the undoped sample is still similar to that of doped sample with $R_F = 0.4$. Therefore, it can be concluded that the degradation pathway of RhB in our system does not change after fluorine doping.

4. Discussion

4.1. Effects of Specific Surface Area on Enhanced Photoactivities. The high activity of photocatalyst was ascribed to a large surface area for adsorbing substrate, small particle sizes to decrease the electron−hole migration distance, and high crystallinity to reduce electron−hole recombination rate.[27,28] On the basis of the results of XRD and TEM, the crystallinity of samples is fine and the particle sizes are almost the same. Thus, the enhanced photoactivies may be assigned to specific surface area. Recently, it has been further confirmed that the expediting photoactivity of TiO_2 coating with SiO_x was attributable to an increase in the amount of adsorption and adsorption strength.[29] However, it is noted that the amounts of adsorbed RhB on $ZnWO_4$ undoped sample and $ZnWO_4$ samples with $R_F = 0.4$ are similar in Figure 8A.

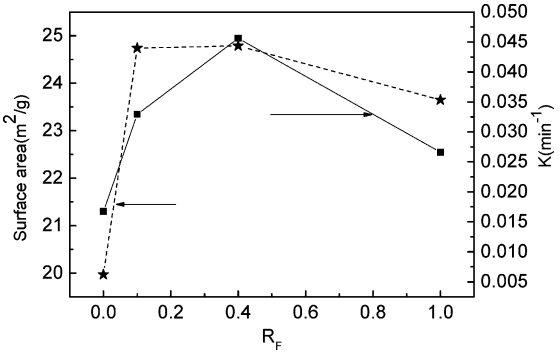

Figure 10. The dependence of the apparent rate constants (k/min^{-1}) and surface areas on fluorine amount for samples at 180 °C for 24 h.

On the other hand, Figure 10 shows the dependence of the apparent rate constants (k/min^{-1}) and specific surface areas on the fluorine-doped concentration of $ZnWO_4$ at 180 °C for 24 h. The solid-style curve represents photocatalytic activities of samples, and the dashed-style curve represents specific surface areas of the as-prepared samples. It can be found that the photocatalytic activities of samples increase with the increase of specific surface area. The sample of $R_F = 0.4$ with the largest surface area (24.8 m^2/g) exhibits the highest photocatalytic activity. However, the sample of $R_F = 0.1$ has a surface area (24.7 m^2/g) similar to that of the sample of $R_F = 0.4$ (24.8 m^2/g), and both of them are far apart in photocatalytic activity.

Therefore, it can be inferred that the specific surface areas played a minor role in enhancing photocatalytic activity in this work.

4.2. Effects of Surface Hydroxyl on Enhanced Photoactivities. Surface hydroxyl is traditionally considered as an important factor affecting the photocatalytic activity.[30] The greater the number of surface hydroxyl groups present on the photocatalyst surface, the faster the photocatalytic reaction.[28] Interestingly, the intensity of surface hydroxyl groups of as-prepared samples are the same in Figure 3A, which elucidated that changing the doping concentration of fluorides does not change the amount of the surface hydroxyls. That is to say, the enhancement of photocatalytic activities for fluorine-doped $ZnWO_4$ catalysts was independent of surface hydroxyl groups in our work.

4.3. Mechanism of Enhanced Photoactivities. On the basis of the above results, the crystallinity, surface area, particle sizes, and surface hydroxyl groups played a minor role in enhancing photocatalytic activity. So what was the main factor affecting the photocatalytic activity of as-prepared samples after fluorine doping?

First, it is known that the photocatalytic activities of semiconductor materials were controlled by the ratio of surface electron transfer rate to the electron−hole recombination rate. If surface electron transfer rate is too fast, it favors the occurrence of the chemical reaction.[1] On the basis of the results of Figure 6, $ZnWO_4$ with $R_F = 0.4$ generated a larger photocurrent than did the undoped $ZnWO_4$ sample. This elucidated that fluorine-ion doping increased the transfer rate of electrons to the photocatalyst surface. So the photogenerated electrons could easily diffuse from the inner regions to the surface of the grains to promote chemical reaction. Therefore, fluorine-doped samples exhibited higher photoactivity than that of undoped samples. This conclusion has also been proved by Hattori et al.[25] However, when the dopant concentration becomes too high ($R_F > 0.4$), the recombination rate will increase because the distance between trapping sites in a particle decreases with the number of dopant ions. This point has also been demonstrated in F^--doped TiO_2.[11]

Second, the rate of the photocatalytic reaction is proportional to $(I_\alpha\Phi)^n$ ($n = 1$ for low light intensity and $n = 1/2$ for high light intensity), where I_α represents the photo numbers adsorbed by photocatalyst per second and Φ is the efficiency of the band gap transition. Therefore, an increase in α (absorption coefficient) or $I_\alpha\Phi$ and a decrease in k_{rec} (rate constant of recombination of the charge carriers) would increase the rate at which the photogenerated electrons reach the surface, leading to effective participation in the surface reaction.[25] The value of α can be calculated from the measured absorbance (A) using the following equation:[11]

$$\alpha = \frac{2.303\rho \times 10^3}{IcM}A$$

where ρ, M, c, and I are density, molecular weight, and molar concentration of $ZnWO_4$, and optical path length, respectively. On the basis of UV-DRS plots in Figure 7, it is clearly seen that the intensity of absorption below 380 nm due to the increase of band gap transition in F^--doped samples as compared to that of in undoped $ZnWO_4$. The enhancement of the photocatalytic activity with F^- doping can be partly explained in terms of an increase in $I_\alpha\Phi$ resulting from intensive absorbance in the UV regions.[11] Therefore, it is reasonable to postulate that the enhancement of the photocatalytic activity with F^--doped $ZnWO_4$ comes from intensive absorbance in the UV regions. The increasing of intensive absorbance resulted in the increase of rate of transfer of photogenerated electrons to the surface, leading to effective participation in the surface reaction.[25]

Consequently, introduction of fluorine can increase the transfer rate of photogenerated electrons to the surface of photocatalysts and then promote photocatalytic activities of $ZnWO_4$ catalyst.

5. Conclusions

A hydrothermal method was developed for the preparation of fluorine interstitial doping of $ZnWO_4$ photocatalysts. The fluorine doping ions could change the coordination sphere around the W atom in the WO_6 octahedron. For the decomposition of RhB, the photocatalytic activity of fluorine-doped $ZnWO_4$ catalysts with $R_F = 0.4$ was increased to 2.6 times. The enhanced photocatalytic activity came from the increase of transfer rate of photogenerated electrons to the photocatalyst surface.

Acknowledgment. This work was partly supported by the Chinese National Science Foundation (20433010205710047) and SRFDP (20060030082).

Supporting Information Available: Photocatalytic reactive system (Figure S1) and 4-chlorophenol photocatalytic degradation over as-prepared samples (Figure S2). This material is available free of charge via the Internet at http://pubs.acs.org.

References and Notes

(1) Hoffmann, M. R.; Martin, S. T.; Chio, W.; Bahnemann, D. W. *Chem. Rev.* **1995**, *95*, 69−96.
(2) Fujishima, A.; Rao, T. N.; Tryk, D. A. *J. Photochem. Photobiol. C: Photochem. Rev.* **2000**, *1*, 1−21.
(3) Zhao, X.; Zhu, Y. F. *Environ. Sci. Technol.* **2006**, *40*, 3367−3372.
(4) Zhao, X.; Yao, W. Q; Wu, Y.; Zhang, S. C.; Yang, H. P.; Zhu, Y. F. *J. Solid State Chem.* **2006**, *179*, 2562−2570.
(5) Fu, H. B.; Lin, J.; Zhang, L. W.; Zhu, Y. F. *Appl. Catal. A: Gen.* **2006**, *306*, 58−67.
(6) Huang, G. L.; Zhang, C.; Zhu, Y. F. *J. Alloys Compd.* **2007**, *432*, 269−276.
(7) Minero, C.; Mariella, G.; Maurino, V.; Pelizzetti, E. *Langmuir* **2000**, *16*, 2632−2641.
(8) Minero, C.; Mariella, G.; Maurino, V.; Vione, D.; Pelizzetti, E. *Langmuir* **2000**, *16*, 8964−8972.
(9) Vohra, M. S.; Kim, S.; Choi, W. *J. Photochem. Photobiol. A: Chem.* **2003**, *160*, 55−60.
(10) Park, H.; Choi, W. *J. Phys. Chem. B* **2004**, *108*, 4086−4093.
(11) Yu, J. C.; Yu, J.; Ho, W.; Jiang, Z.; Zhang, L. *Chem. Mater.* **2002**, *14*, 3808−3816.
(12) Li, D.; Haneda, H.; Hishita, S.; Ohashi, N.; Labhsetwar, N. *J. Fluorine Chem.* **2005**, *126*, 69−77.
(13) Hattori, A.; Yamamoto, M.; Tada, H.; Ito, S. *Chem. Lett.* **1998**, 707−708.
(14) Hattori, A.; Shimoda, K.; Tada, H.; Ito, S. *Langmuir* **1999**, *15*, 5422−5425.
(15) Wang, J. S.; Yin, S.; Zhang, Q. W.; Saito, F.; Sato, T. *J. Mater. Chem.* **2003**, *13*, 2348−2352.
(16) Wang, J. S.; Yin, S.; Zhang, Q. W.; Saito, F.; Sato, T. *Solid State Ionics* **2004**, *172*, 191−195.
(17) Dafinova, R.; Papazova, K.; Bojinova, A. *J. Mater. Sci. Lett.* **1998**, *17*, 237−239.
(18) Nefedov, V. I.; Kokunvo, Y. V.; Buslaev, T. V. *Zh. Neorg. Khim.* **1973**, *18*, 931.
(19) (a) Lesne, J. P.; Caillet, P. *Can. J. Spectrosc.* **1973**, *18*, 69. (b) Formichev, V. V.; Kondratov, O. I. *Spectrochim. Acta* **1994**, *50A*, 1113−1120.
(20) Schofield, P. F.; Knight, K. S.; Redfern, S. A. T.; Cressey, G. *Acta Crystallogr.* **1997**, *B53*, 102−112.
(21) Endo, T.; Kobayashi, T.; Sato, T.; Shimada, M. *J. Mater. Sci.* **1990**, *25* (1B), 619−623.
(22) (a) Park, H.; Choi, W. *J. Phys. Chem. B* **2003**, *107*, 3885. (b) Kim, H. G.; Borse, P. H.; Choi, W.; Lee, J. S. *Angew. Chem., Int. Ed.* **2005**, *44*, 4585.

(23) Butler, M. A. *J. Appl. Phys.* **1977**, *48*, 1914.
(24) Nedilko, S. G.; Hizhnyi, Yu. A.; Nikolaenko. T. N. *Phys. Status Solidi C* **2005**, *2*, 481−484.
(25) Hattori, A.; Tada, H. *J. Sol-Gel Sci. Technol.* **2001**, *22*, 47.
(26) (a) Lei, P. X.; Chen, C. C.; Yang, J.; Ma, W. H.; Zhao, J. C.; Zhang, L. *Environ. Sci. Technol.* **2005**, *39*, 8466−8474. (b) Chen, C. C.; Zhao, W.; Lei, P. X.; Zhao, J. C.; Serpone, N. *Chem. Eur. J.* **2004**, *10*, 1956−1965.
(27) (a) Ohtani, B.; Ogawa, Y.; Nishimoto, S. *J. Phys. Chem. B.* **1997**, *101*, 3746−3752. (b) Li, D.; Haneda, H. *Chemosphere* **2003**, *51*, 129−137. (c) Li, D.; Haneda, H. *J. Photochem. Photobiol. A: Chem.* **2003**, *160*, 203−212.
(28) (a) Ohno, T.; Tokieda, K.; Higashida, S.; Matsumura, M. *Appl. Catal. A: Chem.* **2003**, *244*, 383. (b) Liu, G.; Chen, Z.; Dong, C.; Zhao, Y.; Li, F.; Lu, G. Q.; Cheng, H.-M. *J. Phys. Chem. B* **2006**, *110*, 20823−20828.
(29) Tada, H.; Kubo, Y.; Akazawa, M.; Ito, S. *Langmuir* **1998**, *14*, 2936.
(30) (a) Ding, Z.; Lu, G. Q.; Greenfield, P. F. *J. Phys. Chem. B* **2000**, *104*, 4815. (b) Machado, N. R. C. F.; Santana, V. S. *Catal. Today* **2005**, *595*, 107−108.